High harmonic generation from aligned molecules --amplitude and polarization

Mairesse, Y.; Levesque, J.; Dudovich, N.; Corkum, P.B.; Villeneuve, D.M.

Publisher's version / Version de l'éditeur:
https://doi.org/10.1080/09500340802175766
Journal of Modern Optics, 55, 16, pp. 2591-2602, 2008-09-01

Journal of Modern Optics
Vol. 55, No. 16, 20 September 2008, 2591–2602

Taylor & Francis
Taylor & Francis Group

High harmonic generation from aligned molecules – amplitude and polarization

Y. Mairesse[a,b], J. Levesque[a,c], N. Dudovich[a,d], P.B. Corkum[a,e] and D.M. Villeneuve[a]*

[a]*National Research Council of Canada, Ottawa, Ontario, Canada;* [b]*CELIA, Université Bordeaux I, Talence, France;* [c]*INRS-Énergie et Matériaux, Varennes, Québec, Canada;* [d]*Department of Physics of Complex Systems, Weizmann Institute of Science, Rehovot, Israel;* [e]*University of Ottawa, Ottawa, Canada*

(*Received 13 March 2008; final version received 1 May 2008*)

While high harmonic generation from atoms is relatively well understood, the ability to align gas-phase molecules opens an opportunity to more deeply understand the underlying physics. Many assumptions, such as the single active electron approximation, neglect of the Coulomb potential, the strong field approximation, and the assumption of plane waves, are being challenged by new experimental observations. We study high harmonic emission from aligned molecules such as N_2, O_2 and CO_2. We present experimental measurements of the amplitude of the emission as a function of molecular angle, as well as the polarization state.

Keywords: attosecond; high harmonic generation; molecular alignment

1. Introduction

High harmonic generation (HHG) is a process involving intense femtosecond laser light and gas-phase atoms or molecules [1,2]. The commonly used three-step model [3] provides a semi-classical description of the harmonic generation process. (1) An intense laser field removes the most weakly bound electron. (2) The electron is accelerated by the laser field for about half an optical cycle, and then is driven back to the parent ion. (3) The electron recombines with the parent ion, giving off its energy as an extreme ultraviolet (XUV) photon. If the probabilities of the first two steps can be calibrated, then the XUV spectrum is determined by the transition dipole matrix element that corresponds to the recombination process. Since a wide range of XUV frequencies is generated, the spectrum multiplexes a number of matrix elements in a single measurement.

The quantum mechanical description of HHG is most commonly given by the strong field approximation (SFA) [4]. In the SFA, some of the bound state wave function tunnels through the potential barrier near the peak of the laser field. Once in the continuum, the electron is described by a Volkov wave function. When the continuum wave function returns to the vicinity of the parent ion, it is approximately described by a chirped plane

*Corresponding author. Email: david.villeneuve@nrc.ca

ISSN 0950–0340 print/ISSN 1362–3044 online

DOI: 10.1080/09500340802175766
http://www.informaworld.com

wave [5,6]. This plane wave then interacts with the bound state portion of the wave function, leading to an oscillating charge that radiates electromagnetic radiation.

In either picture, the HHG spectrum is proportional to the square of the recombination dipole matrix element $\boldsymbol{d}$ between the bound state, $\psi_0(\boldsymbol{r})$, and the continuum, $\chi(\boldsymbol{r})$ [7]. The continuum wave function is taken as a plane wave expansion, $\chi(\boldsymbol{r}) = \int a(\varepsilon) \exp[\mathrm{i}\boldsymbol{k}(\varepsilon)\cdot\boldsymbol{r}]\,\mathrm{d}\varepsilon$, where $a(\varepsilon)$ is the complex amplitude of the recombining electron wave packet. The electron kinetic energy ε is related to its wavenumber k by $\varepsilon = k^2/2$ (atomic units are used). The XUV photon frequency Ω is then given by $\Omega = \varepsilon + I_p$, where I_p is the ionization potential. The XUV emission at frequency Ω is proportional to the square of the matrix element $\boldsymbol{d}(\boldsymbol{k}) = \langle\psi_0|\boldsymbol{r}|\boldsymbol{k}\rangle$.

It has been demonstrated in experiments with aligned molecules that the highest occupied molecular orbital (HOMO) largely determines the shape of the HHG spectrum [8]. It was shown [9] that the process of high harmonic generation could be used to form an image of a single electron orbital wave function of N_2, and that the orbitals of rare gas atoms determine the HHG spectrum [6]. These experiments are supported by calculations that show the dependence on the HOMO [10–13]. In this paper we will show that the HHG spectra from aligned N_2, O_2 and CO_2 have unique features that are determined by the electronic structure of each molecule.

Harmonic generation from aligned molecules has forced us to re-examine the theory of HHG. A decade ago, the strong field approximation [4] was considered completely adequate to explain HHG. Recently, a number of the underlying approximations and assumptions have been challenged. For example, multi-electron effects have now been included [14,15]. The plane wave assumption has been challenged, by forcing the continuum wave function to be orthogonal to bound states [15], or by using the Eikonal–Volkov Approximation (EVA) to include corrections due to the effective potential of the molecule [16,17]. We hope that the measurements presented in this paper will inspire theoreticians to continue to improve the models of HHG from molecules.

2. Amplitude response of aligned molecules

The experimental setup, shown in Figure 1, has been described previously [9,18]. Briefly, N_2, O_2 or CO_2 gas was introduced into the vacuum chamber through a pulsed supersonic valve providing a gas density of about 10^{17} cm^{-3} with a rotational temperature of about 30 K. A 30 fs duration, 800 nm laser pulse with an intensity of about 5×10^{13} W cm^{-2} created a superposition of rotational states, leading to periodic revivals of molecular alignment [19,20]. The direction along which the molecular axes were aligned could be rotated by means of a half wave plate. At the peak of the rotational revival, typically 4–20 ps after the first pulse, a second, more intense, laser pulse was focused into the gas to produce high harmonics. Its intensity was $\sim 1-2 \times 10^{14}$ W cm^{-2}. The HHG spectra were recorded by an XUV spectrometer consisting of a variable groove spacing grating and an MCP and CCD camera.

HHG spectra were recorded for molecules aligned in 5° steps in the range of $\pm 100°$ relative to the intense laser's polarization. The results are presented in Figure 2. The value that is plotted is related to the measured intensity of each harmonic order, $S(\Omega)$, as follows.

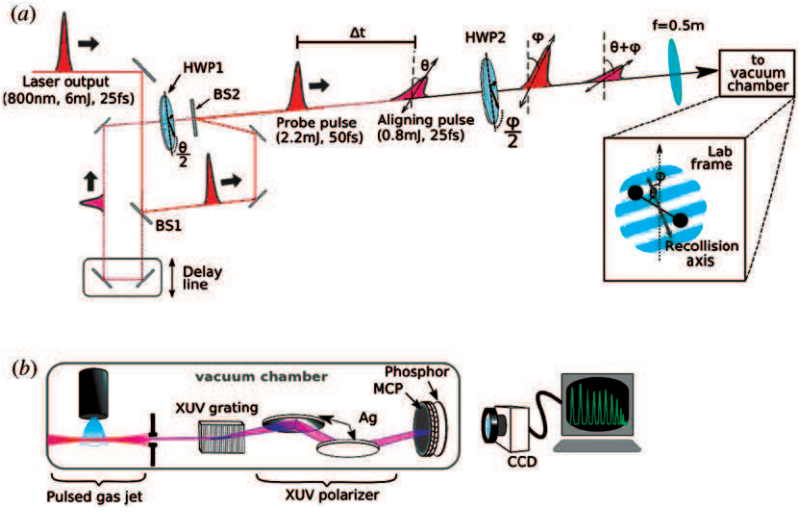

Figure 1. Diagram of the experimental setup. (*a*) The Ti:Sa laser pulse is split into two pulses whose polarization can be controlled independently by rotating two half waveplates HWP1 and HWP2. The first pulse aligns the molecular sample along its polarization axis, and the second delayed pulse produces high harmonics during a fractional revival of the rotational wavepacket. (*b*) The XUV emission is recorded with a spectrometer that consisted of a Hitachi variable groove spacing 1200 line mm^{-1} grating, a microchannel plate (MCP) and phosphor screen, a CCD camera and computer to capture the images. The spectrometer could also optionally include a pair of silver mirrors that serve as polarizers. (The color version of this figure is included in the online version of the journal.)

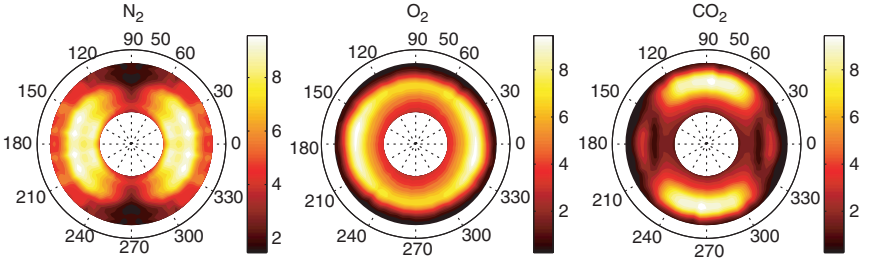

Figure 2. Experimental high harmonic spectra versus angle between the molecular axis and the laser polarization, from N_2, O_2 and CO_2 molecules. The color scale is the square root of the intensity of each harmonic, divided by the continuum wave function amplitude $\Omega^2 a(\Omega)$. The radius in the polar plot is the harmonic order (17–43), and the polar angle is the angle between the molecular axis and the laser polarization. (The color version of this figure is included in the online version of the journal.)

In the three step model, the HHG response is a product of the ionization, the propagation, and the recombination. We lump together the first two steps into a term that describes the continuum wave function at the time of recombination, $a(\Omega)$. The emitted signal $S(\Omega)$ is given by

$$S(\Omega) = \Omega^4 \left| a(\Omega) D(\Omega) \right|^2. \tag{1}$$

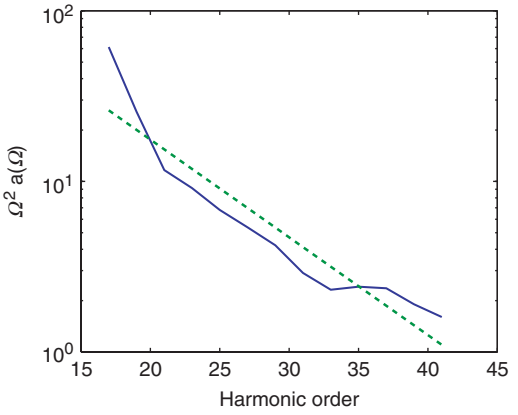

Figure 3. Calibration of the continuum wave function $\Omega^2 a(\Omega)$ amplitude from the reference argon spectrum. The HHG spectrum of argon is recorded, then is divided by the calculated recombination dipole for the Ar 3p orbital. A straight line fit on the semilog scale is used to normalize the spectra presented in Figure 2. (The color version of this figure is included in the online version of the journal.)

Here, Ω is the emitted XUV frequency, and D is the recombination dipole matrix element. The spectral amplitude of the continuum wave function $a(\Omega)$ was determined by a separate measurement of the harmonic spectrum, $S_{\text{ref}}(\Omega)$, taken from a reference atom, argon. Rather than matching the ionization potential of the molecules with individual reference atoms, we used only argon. It was shown in [6] that atoms as different as He, Ne and Ar, gave essentially the same continuum wave function amplitude.

$$a(\Omega) = \frac{S_{\text{ref}}(\Omega)^{1/2}}{\Omega^2 D(\Omega)}.$$

D is evaluated using the 3p orbital of argon calculated by GAMESS [21].

The calibration $\Omega^2 a(\Omega)$ is approximately a straight line on a semilog plot [6] as shown in Figure 3. We fit it to a linear function, $\Omega^2 a(\Omega) = a_1 \exp(-a_2\Omega)$, to avoid any small deviations due to structure in the argon spectrum, for example a suspected Cooper minimum near H31 [22]. Thus, in Figure 2 we plot $S(\Omega)^{1/2} / (\Omega^2 a(\Omega))$.

It should be noted that the alignment dependence of the ionization probability is implicitly included in these measurements. For example, we know that N_2 is more easily ionized parallel to its molecular axis, whereas CO_2 and O_2 preferentially ionize at 45° [23]. In addition, all values are integrated over the distribution of molecular angles that are present in the aligned ensemble.

Each molecule is clearly distinctive, supporting our notion that the electronic structure of each molecule is responsible for the HHG emission. N_2 shows strongest emission near 0°, whereas CO_2 is strongest at 90°. O_2 shows less variation with angle, but peaks broadly near 0°.

The CO_2 measurements clearly show an amplitude minimum near 0° that is conventionally attributed to two-center interference in the emission process [24–26]. The position of the minimum goes to higher order with increasing molecular angles, as

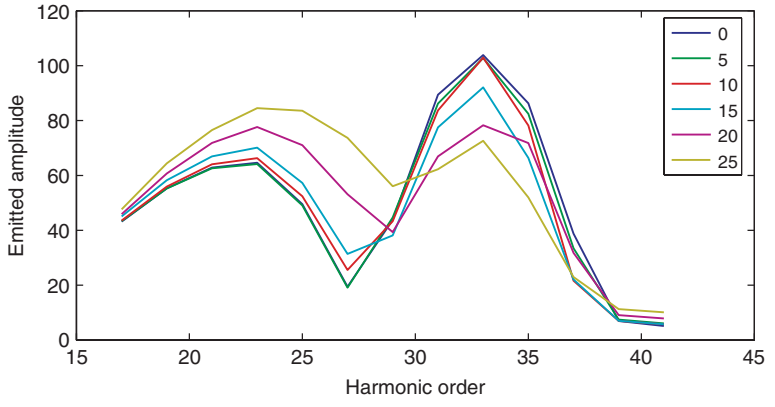

Figure 4. Lineouts of the high harmonic spectra for CO_2 that were presented in Figure 2, for a few angles near 0°. The minimum at H27 is seen to shift to higher orders as the molecule is rotated. This minimum is associated with two-center interference of emission from the two oxygen atoms. (The color version of this figure is included in the online version of the journal.)

seen in Figure 4. For the simple plane wave model, destructive interference of emission from each of the oxygen atoms occurs when $\sin(k \cdot R/2) = 0$, where $R = 2.3$ Å is the distance between the oxygen atoms, and k is the electron wavenumber (or momentum in atomic units) associated with the harmonic order. This can be written as $\cos\theta_{\mathrm{mol}} = 2\pi/kR$. For $\theta_{\mathrm{mol}} = 0$, the minimum should occur at H27, assuming the 'dispersion relation' $\Omega = k^2/2 + I_p$. Measurements of the harmonic phase by the RABBITT technique [27] show a phase jump of about 2 rad in this region, and the position of the phase jump increases with molecular angle. These observations seem consistent with a two-center interference process that depends on molecular orientation. However, it should be noted that there is some disagreement in the location of the interference minimum. Kanai et al. [26] observed the minimum at H25, where Vozzi et al. [25] observed it at H33. This discrepancy seems to be attributed to an intensity dependence of the interference that is not predicted by the simple model and needs further theoretical investigation.

The N_2 measurements show a minimum around H25. This is seen more clearly in Figure 5, which comes from a different data set [9] than that in Figure 2. Interestingly, this minimum does not shift to higher orders as the molecule is rotated away from the laser polarization, and even exists in unaligned molecular samples. Measurements of the harmonic phase in randomly aligned [28] and aligned N_2 [27] show a phase jump starting at H25, also independent of angle. All these observations are in contradiction with the simple two-center interference model, which predicts a strong angular dependence of the amplitude and phase. We believe that this discrepancy is due to multi-electron effects in the generation process.

3. Polarization of emission

In order to measure the polarization state of the emitted XUV radiation, the previous setup was modified to include a pair of silver mirrors at 20° and 25° angles between the

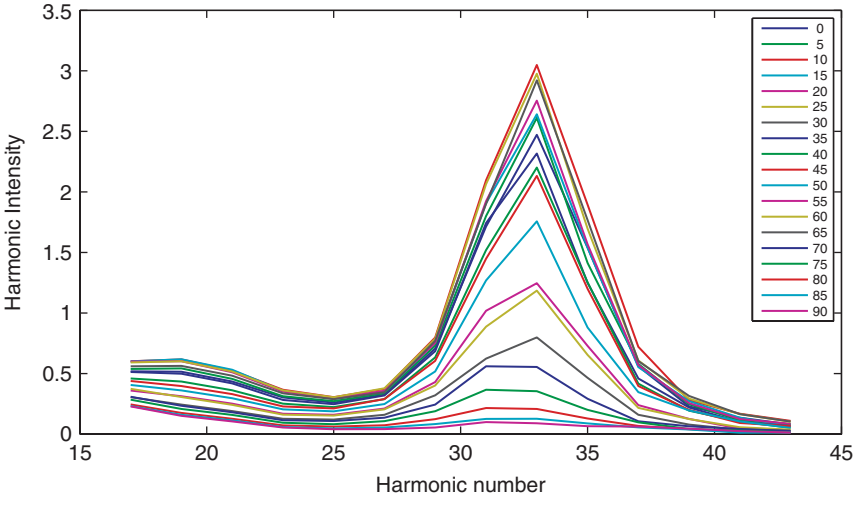

Figure 5. The HHG spectra from aligned N_2 molecules for angles between 0 and 90°. These spectra have been normalized by the argon reference spectrum. A clear minimum at H25 exists for all angles. (The color version of this figure is included in the online version of the journal.)

grating and the MCP, as seen in Figure 1(*b*) [29]. These mirrors acted as an XUV polarizer [30], although not with perfect extinction. As in the previous section, the direction of the molecular axis could be controlled by waveplate HWP1, and was varied in 5° steps over the range ±100°. In addition, the polarization of both pump and probe pulses was rotated by HWP2. In a typical polarimetry measurement, the analyzing polarizer is rotated; in the present case we keep the analyzer fixed and rotate both the molecules and the probe laser polarization. Further details of the experimental setup can be found in [29].

Figure 6 shows how the polarization state was determined experimentally. The selectivity of the polarizer was individually calibrated for each harmonic order by recording the signal for argon, for which the polarization should be linear.

The results of the polarization measurement for different aligned molecules are shown in Figure 7. The convention used for the sign of the polarization angle is shown in Figure 8. We present the polarization direction in the laboratory frame, in which the incoming laser polarization is vertical. It is also possible to present the same data in the molecular frame (not shown). Lineouts at specific molecular angles are shown in Figure 9. As was the case for the measurement of harmonic intensity, each molecule shows a unique signature.

The polarization rotation measured in O_2, shown in Figure 7(*b*), is rather unremarkable compared with the other molecules studied. The XUV polarization is rotated in the direction of the molecular axis, but its value is largely independent of molecular angle or harmonic order. This implies that there is no change of sign of the recombination dipole vector components.

The polarization measurements for CO_2 molecules are shown in Figure 7(*c*). This molecule shows the greatest amount of polarization rotation of the three molecules studied. It is significant that the direction is opposite to that of O_2. The maximum rotation coincides with the harmonic order previously associated with a minimum in the harmonic

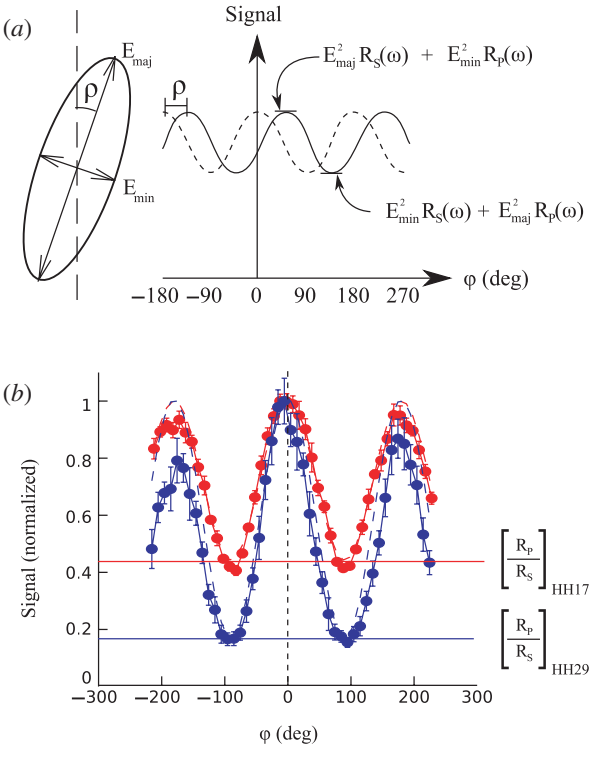

Figure 6. Schematic of how to measure the polarization state of light using an imperfect polarizer. (*a*) The incoming radiation is characterized by the major and minor axes of the polarization ellipse, and the rotation angle ρ of the major axis from a reference direction. By rotating the analyzing polarizer and recording the transmitted signal, a sinusoidal variation is recorded. The peak to valley ratio determines the major to minor ellipse ratio, while the offset from zero determines the rotation ρ of the ellipse. (*b*) The recorded signal is shown for harmonics 17 and 29 in argon. The emission from argon will be linearly polarized parallel to the probe laser polarization, and serves as a calibration of the polarizer. Each harmonic order was individually calibrated in this manner. (The color version of this figure is included in the online version of the journal.)

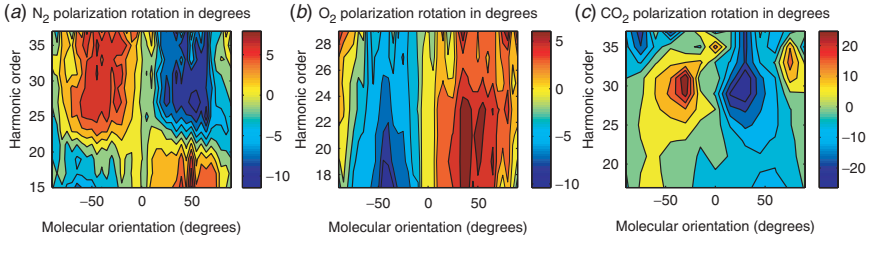

Figure 7. Measurement of the polarization rotation of harmonics produced in aligned N_2, O_2 and CO_2. The color represents the rotation angle from vertical in degrees. Positive values (color red) mean that the emitted XUV polarization has deviated from the probe laser polarization direction, in the direction of the molecular axis. For an atom, the rotation angle will be zero. To within experimental accuracy, the emitted radiation was linearly polarized. (The color version of this figure is included in the online version of the journal.)

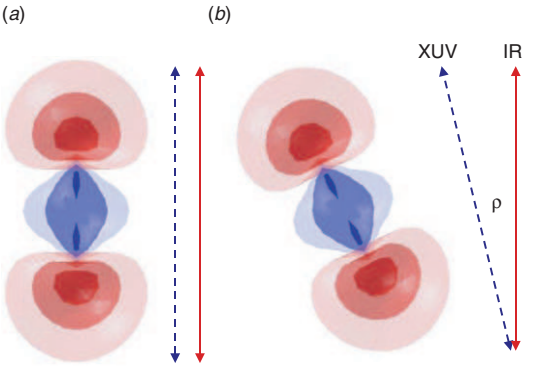

Figure 8. A cartoon showing the convention used for the rotation angle. When the molecular axis is parallel to the incoming laser polarization (red, solid line), the emitted XUV radiation (blue, dashed line) by symmetry must be polarized parallel to it. When the molecule is rotated, the two polarizations no longer need to be parallel. The XUV polarization can follow in the direction of the molecular axis (positive ρ) as shown, or in the opposite direction (negative ρ). (The color version of this figure is included in the online version of the journal.)

spectrum in CO_2. Thus, polarimetry allows us to attribute this amplitude minimum to the component of the dipole moment that is parallel to the generating laser polarization.

The N_2 molecules in Figure 7(*a*) show a change in behavior between low and high harmonic orders. For the low harmonics, the polarization direction rotates in the direction of the laser polarization. The high harmonics show a rotation in the opposite direction. This remarkable feature was recently confirmed by other measurements [31]. The point at which the rotation changes sign is around H21, and this point is largely independent of angle. This almost coincides with the order at which the emission amplitude has a minimum, H25, which is also independent of angle. The minimum in amplitude indicates a minimum in the recombination dipole matrix element. The change in polarization direction indicates a sign change in the perpendicular component of the vector recombination dipole. This would seem to be contrary to the conclusion from the experimental measurements in which it seems that the perpendicular component changes sign. However, the experimental results are consistent with the model interpretation where the parallel component changes sign. Since the experiment only measures the angle of the polarization modulo π, what seems like a rotation of say 20° could in reality be a rotation of -160°. Thus, the amplitude and polarization measurements contain complementary information about the recombination dipole.

Present models of the harmonic generation process are not sophisticated enough to fully use this information. The best that we can do is to predict the polarization based on current models. We base our analysis on a multi-electron version of the strong-field approximation. We take x as the laser polarization axis. The momentum of the free electron, k, is also along x. The molecule lies in the xy-plane. Since the re-collision electron is the same for both polarizations, we can ignore the re-collision amplitude and phase, and concentrate on the dipole contribution.

We approximate the continuum electron by a set of plane waves, $\psi_k = \exp(\mathrm{i}kx)$ for each electron wavenumber k which is in turn determined by the observed harmonic frequency Ω

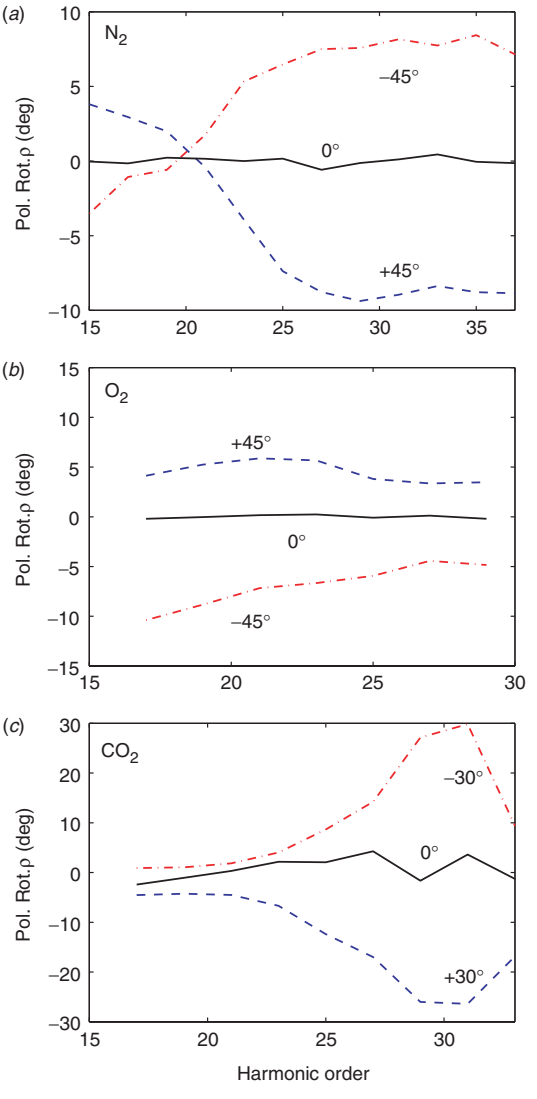

Figure 9. Measured values of $\rho(\omega)$, the rotation of the polarization axis from the driving laser's polarization axis, for harmonics generated in (*a*) N_2 aligned at 0° and ±45°, (*b*) O_2 aligned at 0° and ±45° and (*c*) CO_2 aligned at 0° and ±30°. Here ρ represents the angle between the laser polarization axis and the polarization of the emitted XUV harmonics. Positive ρ means that the XUV polarization has rotated in the direction of the molecular axis. These cuts are taken from the data presented in Figure 7. (The color version of this figure is included in the online version of the journal.)

by $\Omega = k^2/2 + I_p$ and I_p is the ionization potential of the molecule. The transition dipole is given by [9]

$$\boldsymbol{d}(k;\theta) = \langle \psi_0(\boldsymbol{r};\theta)|\boldsymbol{r}|\exp(\mathrm{i}kx)\rangle. \tag{2}$$

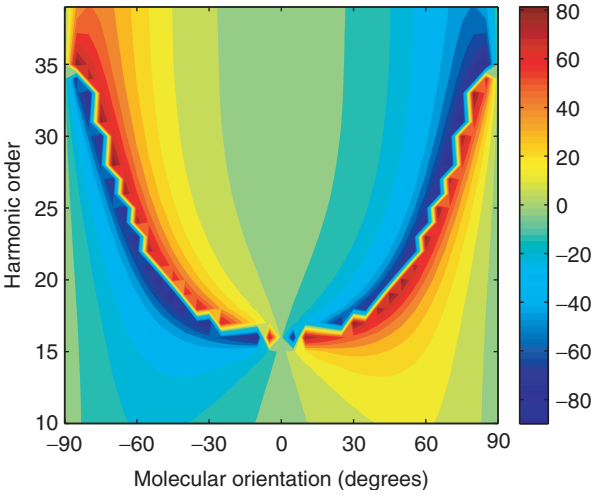

Figure 10. Calculated direction of polarization from aligned N_2 molecules as a function of molecular orientation. Molecular orbitals are calculated using GAMESS and a cc-pVTZ basis set. The model assumes a plane wave continuum and includes indistinguishability of electrons upon recombination. Although it predicts a greater polarization rotation than was observed experimentally, the trend is similar. For example, the model predicts a positive polarization rotation for low harmonics, then a negative rotation for higher harmonics. (The color version of this figure is included in the online version of the journal.)

Here the notation $\psi_0(\boldsymbol{r}; \theta)$ refers to the ground state wavefunction rotated by an angle θ from the x-axis in the laboratory frame. Angle θ corresponds to the horizontal axis labeled 'Molecular Orientation' in Figure 7 and the angles in Figure 9. (We also include additional terms, not shown, due to multi-electron effects upon recombination [14,32].) The transition dipole is a vector quantity with components d_x and d_y. The direction defined by this dipole corresponds to the direction of the polarization axis that we measure experimentally.

This model predicts that the XUV should be linearly polarized for all the molecules used, as was observed. Any orbital with inversion symmetry will have the same phase for both components, because each axis has the same symmetry.

The calculated $\rho = \arctan(d_y/d_x)$, using the $3\sigma_g$ HOMO of N_2 calculated by GAMESS [21] using a cc-pVTZ basis set, is shown in Figure 10. The theoretical calculation shows some qualitative agreement with the experiment in Figure 7 for N_2. The model predicts a positive rotation of the polarization for low harmonics, then a flip in the direction for higher harmonics. For example, the polarization rotation for a molecular angle of 30° goes from 20° at H15 to −20° at H35, similar to the experimental measurement. The model predicts that the polarization direction flips almost 180° in between, something that cannot be resolved in the experiment. This suggests that the parallel component of the dipole is changing sign, not the perpendicular component. However, the model fails to predict the invariance of the harmonic order at which this sign change occurs. The parabolic shape along which the polarization changes direction depends on the details of the model. Using a single $3\sigma_g$ orbital yields a narrow parabola, whereas including electron exchange between all seven orbitals makes the parabola wider. Similarly, using a simple 6-31G basis

set for the quantum chemistry calculation gives a narrower parabola than does a more sophisticated cc-pVTZ basis set. However, the model still fails to predict the flat line seen in the experiment.

4. Conclusion

We have measured the amplitude and polarization state of high order harmonics generated from aligned N_2, O_2 and CO_2 molecules. Very different features were observed, which confirms the high sensitivity of the harmonic emission to molecular structure. We have shown that present models of high harmonic generation fail to reproduce robust experimental observations. In CO_2 there is a minimum in the parallel component of the dipole moment that shifts to higher orders as the molecules are rotated away, in good agreement with the two-center interference model. However, the position of this minimum depends on the laser intensity, which is not explained by current models. In N_2, the minimum in the harmonic spectrum does not shift as the molecular orientation is changed, which is also in contradiction with theoretical predictions. It was recently shown that the polarization of high harmonics is expected to encode signatures of non-adiabatic multi-electron dynamics [33] and we hope that the results presented here will trigger further theoretical investigations.

References

[1] Scrinzi, A.; Ivanov, M.Y.; Kienberger, R.; Villeneuve, D.M. *J. Phys. B* **2006,** *39,* R1–R37.
[2] Corkum, P.B.; Krausz, F. *Nat. Phys.* **2007,** *3,* 381–387.
[3] Corkum, P.B. *Phys. Rev. Lett.* **1993,** *71,* 1994–1997.
[4] Lewenstein, M.; Balcou, P.; Ivanov, M.Y.; L'Huillier, A.; Corkum, P.B. *Phys. Rev. A* **1994,** *49,* 2117–2132.
[5] Mairesse, Y.; de Bohan, A.; Frasinski, L.J.; Merdji, H.; Dinu, L.C.; Monchicourt, P.; Breger, P.; Kovacev, M.; Taïeb, R.; Carré, B., et al. *Science.* **2003,** *302,* 1540–1543.
[6] Levesque, J.; Zeidler, D.; Marangos, J.P.; Corkum, P.B.; Villeneuve, D.M. *Phys. Rev. Lett.* **2007,** *98,* 183903.
[7] Bethe, H.A.; Salpeter, E.E. *Quantum Mechanics of One- and Two-electron Atoms;* Springer: Berlin, 1957.
[8] Torres, R.; Kajumba, N.; Underwood, J.G.; Robinson, J.S.; Baker, S.; Tisch, J.W.G.; de Nalda, R.; Bryan, W.A.; Velotta, R.; Altucci, C., et al. *Phys. Rev. Lett.* **2007,** *98,* 203007.
[9] Itatani, J.; Levesque, J.; Zeidler, D.; Niikura, H.; Pépin, H.; Kieffer, J.C.; Corkum, P.B.; Villeneuve, D.M. *Nature.* **2004,** *432,* 867–871.
[10] Zhou, X.X.; Tong, X.M.; Zhao, Z.X.; Lin, C.D. *Phys. Rev. A* **2005,** *71,* 061801(R)-1–4.
[11] Zhou, X.X.; Tong, X.M.; Zhao, Z.X.; Lin, C.D. *Phys. Rev. A* **2005,** *72,* 033412-1–7.
[12] Morishita, T.; Le, A.-T.; Chen, Z.; Lin, C.D. *Phys. Rev. Lett.* **2008,** *100,* 013903.
[13] Lein, M. *J. Phys. B* **2007,** *40,* R135–R173.
[14] Patchkovskii, S.; Zhao, Z.; Brabec, T.; Villeneuve, D.M. *Phys. Rev. Lett.* **2006,** *97,* 123003.
[15] Santra, R.; Gordon, A. *Phys. Rev. Lett.* **2006,** *96,* 073906.
[16] Smirnova, O.; Spanner, M.; Ivanov, M.Yu. *J. Phys. B* **2006,** *39,* S307–S321.
[17] Smirnova, O.; Spanner, M.; Ivanov, M.Yu. *J. Phys. B* **2006,** *39,* S323–S339.

[18] Itatani, J.; Zeidler, D.; Levesque, J.; Spanner, M.; Villeneuve, D.M.; Corkum, P.B. *Phys. Rev. Lett.* **2005,** *94,* 123902.
[19] Rosca-Pruna, F.; Vrakking, M.J.J. *Phys. Rev. Lett.* **2001,** *87,* 153902-1–4.
[20] Dooley, P.W.; Litvinyuk, I.; Lee, K.F.; Rayner, D.M.; Spanner, M.; Villeneuve, D.M.; Corkum, P.B. *Phys. Rev. A* **2003,** *68,* 023406-1–12.
[21] Schmidt, M.; Baldridge, K.; Boatz, J.; Elbert, S.; Gordon, M.; Jensen, J.; Koseki, S.; Matsunaga, N.; Nguyen, K.; Su, S., et al. *J. Comput. Chem.* **1993,** *14,* 1347–1363.
[22] Cooper, J.W. *Phys. Rev.* **1962,** *128,* 681–693.
[23] Pavičić, D.; Lee, K.F.; Rayner, D.M.; Corkum, P.B.; Villeneuve, D.M. *Phys. Rev. Lett.* **2007,** *98,* 243001.
[24] Lein, M.; Hay, N.; Velotta, R.; Marangos, J.P.; Knight, P.L. *Phys. Rev. A* **2002,** *66,* 023805-1–6.
[25] Vozzi, C.; Calegari, F.; Benedetti, E.; Caumes, J.-P.; Sansone, G.; Stagira, S.; Nisoli, M.; Torres, R.; Heesel, E.; Kajumba, N., et al. *Phys. Rev. Lett.* **2005,** *95,* 153902.
[26] Kanai, T.; Minemoto, S.; Sakai, H. *Nature* **2005,** *435,* 470–474.
[27] Boutu, W. *Nat. Phys.* **2008,** *4*, 545–549.
[28] Wabnitz, H.; Mairesse, Y.; Frasinski, L.J.; Stankiewicz, M.; Boutu, W.; Breger, P.; Johnsson, P.; Merdji, H.; Monchicourt, P.; Salières, P., et al. *Eur. Phys. J. D* **2006,** *40,* 305–311.
[29] Levesque, J.; Mairesse, Y.; Dudovich, N.; Pépin, H.; Kieffer, J.-C.; Corkum, P.B.; Villeneuve, D.M. *Phys. Rev. Lett.* **2007,** *99,* 243001.
[30] Antoine, P.; Carré, B.; L'Huillier, A.; Lewenstein, M. *Phys. Rev. A* **1997,** *55,* 1314–1324.
[31] Mairesse, Y.; Haessler, S.; Fabre, B.; Higuet, J.; Boutu, W.; Breger, P.; Constant, E.; Descamps, D.; Mével, E.; Petit, S., et al. *New J. Phys.* **2008,** *10,* 025028-1–11.
[32] Patchkovskii, S.; Zhao, Z.; Brabec, T.; Villeneuve, D.M. *J. Chem. Phys.* **2007,** *126,* 114306.
[33] Zhao, Z.; Yuan, J.; Brabec, T. *Phys. Rev. A* **2007,** *76,* 031404-1–4.